JACS
JOURNAL OF THE AMERICAN CHEMICAL SOCIETY
pubs.acs.org/JACS
Communication

Nickel(II) Metal Complexes as Optically Addressable Qubit Candidates

Michael K. Wojnar, Daniel W. Laorenza, Richard D. Schaller, and Danna E. Freedman*

Cite This: J. Am. Chem. Soc. 2020, 142, 14826−14830
Read Online
ACCESS | Metrics & More | Article Recommendations | Supporting Information

ABSTRACT: The inherent atomic level structural control of synthetic chemistry enables the creation of qubits, the base units of a quantum information science system, designed for a target application. For quantum sensing applications, enabling optical read-out of spin in tunable molecular systems, akin to defect-based systems, would be transformative. This approach would bring together molecular tunability with optical read-out technology. In theory, nickel ions in octahedral symmetry meet all the criteria for optical readout of spin. Yet, to the best of our knowledge, there are no pulse EPR studies on Ni^{2+} molecules. We identified two compounds featuring highly symmetric Ni^{2+} centers, thereby engendering weak zero-field splitting to enable EPR addressability: $[Ni(phen)_3](BF_4)_2$ (**1**) and $[Ni(pyr_3)_2](BF_4)_2$ (**2**) (phen = 1,10-phenanthroline; pyr_3 = tris-2-pyridyl-methane). Crucially, these complexes feature the requisite strong field ligands to enable emission for optical addressability. We extracted axial zero-field splitting parameters of D = +0.9 cm^{-1} and +2.7 cm^{-1} for **1** and **2**, respectively, enabling pulse EPR measurements. Both compounds produce emission at λ_{max} = 938−944 nm. The aggregate of these results expands the catalogue of qubit materials to Ni^{2+}-based compounds and offers a future pathway for optical readout of these molecules.

Quantum information science (QIS) is an emerging paradigm, whereby inherent quantum properties of an object are harnessed for quantum applications including communication, sensing, and metrology.[1−7] In QIS systems, bottom-up design of paramagnetic spin centers as quantum bits, or qubits, provides immense control over the electronic structure and environment of the qubit.[8] Such synthetic tunability has enabled control over coherence times,[9,10] design of multiqubit systems for gate operations,[11,12] and integration of qubits into diverse device architectures and scalable arrays.[13−16] To realize the promise of an atomistic approach to QIS, we need a generalizable readout strategy. Optically addressable solid-state spins provide an enticing framework for readout of molecular systems. One of the most well-studied optically addressable quantum sensor candidates is the anionic nitrogen-vacancy (NV) center, a defect in diamond in which a nitrogen atom substitutes for a carbon atom with an adjacent vacancy.[17,18] This defect hosts an S = 1 ground state, which is optically initialized and read out under off-resonant optical excitation. While the NV centers are the most developed system with these properties, transition metal dopants in wide band gap semiconductors, such as chromium or vanadium in silicon carbide (Cr^{4+}/V^{4+}:SiC),[19,20] as well as rare-earth ions in garnet host crystals,[21−23] have demonstrated an optical initialization and readout mechanism using resonant excitation. This wide array of defect-based systems that supports optical readout offers promise to extend this approach beyond defects to structurally precise materials such as molecules.

A bottom-up design through chemical synthesis allows us to merge the optical addressability of solid-state defects with the tunability of chemical synthesis. Our goal is the replication of the electronic structure of these defect sites via coordination chemistry. Specifically, we need a system that features EPR addressability and optical emission. Recently, we demonstrated success with this bottom-up strategy to create optically addressable molecular qubits in a series of Cr^{4+} transition metal complexes.[24] The combination of strong field aryl ligands coordinated to Cr^{4+} in a high symmetry configuration allowed for a spin-optical interface with atomistic control. Expanding to other transition metals enables tunable emission and control of the local environment to create designer qubits targeted for specific sensing or communication applications. To realize optical read-out, we need an S = 1 ground state featuring weak zero-field splitting to enable microwave manipulation coupled with strong field ligands to ensure the lowest lying excited state is a singlet that radiatively decays to the ground state.[25]

One class of inorganic complexes that meet these criteria are divalent nickel ions in octahedral coordination geometries containing polypyridine ligands. The O_h geometry around nickel leads to an S = 1 ground state, in which two unpaired d electrons reside in the antibonding e_g set of d orbitals. Polypyridine ligands impart a strong ligand field around the nickel ion to ensure an S = 0 first excited state.[26,27] While Ni^{2+} is an attractive target, it is typically considered "EPR-silent",[28] with few examples of pulse EPR data.[29,30] High-symmetry, octahedral environments support the small zero-field splitting values (denoted by the parameters D and E) required for spin

Received: June 26, 2020
Published: August 10, 2020

https://dx.doi.org/10.1021/jacs.0c06909
J. Am. Chem. Soc. 2020, 142, 14826−14830

manipulation.[31,32] Herein we report the optical, magnetic, and pulse EPR analyses of two air- and water-stable Ni^{2+} complexes, $[Ni(phen)_3](BF_4)_2$ (**1**) and $[Ni(pyr_3)_2](BF_4)_2$(**2**) (phen = 1,10-phenanthroline; pyr_3 = tris-2-pyridyl-methane) (Figure 1). Notably, both **1** and **2** meet the requirements for

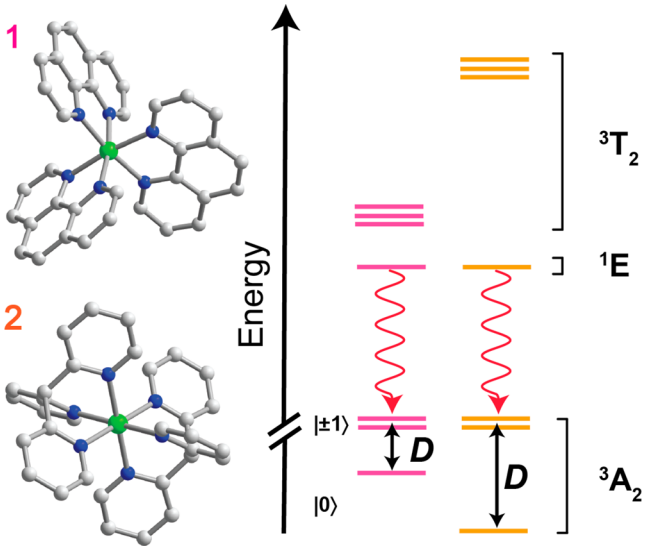

Figure 1. (Left) Molecular structure of $[Ni(phen)_3]^{2+}$ (**1**) and $[Ni(pyr_3)_2]^{2+}$ (**2**) as found in the crystal structure. Green, blue, and gray spheres represent Ni, N, and C atoms, respectively. (Right) Energy-level diagram for **1** and **2**.

molecular optically addressable qubits, including the correct ground- and excited-state manifold, and an emissive component to provide an optical interface to the spin component.

To ensure an EPR-accessible transition, we sought compounds featuring a rigorously octahedral ligand field with strong donors. The strength of the donors increases the energy separation between the d_{xy} and $d_{x^2-y^2}$ orbitals, which is inversely proportional to axial zero-field splitting.[33] As D originates from the coupling of electronic ground states to excited states via spin−orbit coupling, the strong field polypyridine ligands were a crucial design principle to offset the large spin−orbit coupling constant (630 cm^{-1})[34] of Ni^{2+} and lead to EPR-addressable complexes. Toward that end, compounds **1** and **2** were synthesized following modifications of the literature procedures.[35,36]

To assess the EPR addressability of nickel in these strong field coordination environments, we employed multifrequency cw-EPR spectroscopy (Figure 2), which demonstrated these molecules feature an S = 1 ground state. This enabled quantification of the axial and rhombic zero-field splitting parameters, D and E. The observed spectra were modeled with EASYSPIN and the spin Hamiltonian, $\hat{H} = D\hat{S}_z^2 + (E(\hat{S}_x^2 - \hat{S}_y^2) + \sum g_i \mu_B \boldsymbol{HS} + \boldsymbol{IAS}$, which provides the energies of the M_S levels for the spin $\boldsymbol{S}$ as a function of D and E as well as the applied dc magnetic field ($\boldsymbol{H}$). In this Hamiltonian, $\hat{S}_i$ ($i = x, y,$ and z) are the spin operators, g_i ($i = x, y,$ and z) are the g factors, $\boldsymbol{I}$ is the nuclear spin of the ^{14}N nucleus, $\boldsymbol{A}$ is the hyperfine coupling tensor, and μ_B is the Bohr magneton. The best simulations for **1** and **2** yielded the values shown in Table 1. The magnitudes of the zero-field splitting parameters in **1** and **2** confirm the EPR addressability of the complexes. Interestingly, $|D|$ increases slightly upon moving to the pyr_3 ligand. Whereas

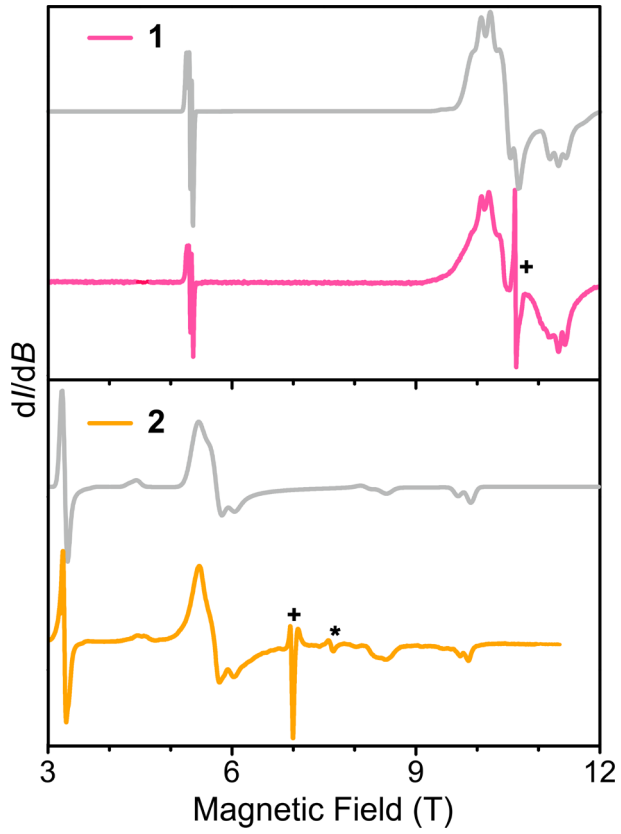

Figure 2. High frequency EPR spectra for **1** (318.7 GHz) and **2** (213.0 GHz) with their best simulations (gray spectra) at 5 K (+ denotes the double quantum transition; * denotes a g = 2 impurity).

Table 1. Simulated Spin Hamiltonian Parameters for 1 and 2

	g_x	g_y	g_z	D (cm^{-1})	$\lvert E\rvert$ (cm^{-1})	$A_\perp$ (^{14}N) (MHz)	$A_\parallel$ (^{14}N) (MHz)
1	2.140	2.100	2.182	+0.90	0.20	3.2	3.8
2	2.160	2.150	2.140	+2.70	0.10	4.0	7.0

the stronger ligand field should lessen the excited state contribution to D, we hypothesize that the other low-lying excited states (i.e., ^1E) lead to this increase.

Zeeman diagrams based on the cw-EPR spectra reveal the identity of the EPR transitions and the ground-state energy level scheme for **1** and **2** (Figures S6 and S8). This Zeeman diagram changes slightly for a field aligned along the x- and y-axes of the molecule due to the different principal g-values. For both systems, a sharp resonance is observed at low fields, assigned to the forbidden half-field transition (ΔM_S = 2), which is characteristic of an S = 1 ground-state spin, while the multiple transitions observed at higher fields correspond to allowed ΔM_S = 1 transitions. For **2**, with larger zero-field splitting values, the resonances are also spread over a larger field range. The energy level schemes illustrate the ground-state chemical engineering afforded to the magnetic properties of molecules in **1** and **2**.

We employed pulse W-band high-power EPR (HiPER) spectroscopy[37,38] to evaluate the coherence properties of **1** and **2**. All pulse EPR experiments were performed on 1 mM solutions in 1:1 H_2O/glycerol solutions. We first measured the echo-detected field-swept (EDFS) spectra for **1** and **2** by

https://dx.doi.org/10.1021/jacs.0c06909
J. Am. Chem. Soc. 2020, 142, 14826−14830

applying a two-pulse Hahn-echo detection sequence ($\pi/2$-τ-π-τ-echo) at a fixed τ value while sweeping the magnetic field. The resultant EDFS spectrum of **1** exhibits an intense and broad transition at 3.00 T and a less intense yet sharp transition at 1.53 T. Similarly, **2** shows a sharp peak at 0.00 T, with three broad peaks at higher magnetic fields (0.69, 3.00, and 6.00 T in Figure S10). The EDFS spectra for **1** and **2** are consistent with predicted spectra at W-band frequency based on the magnetic parameters obtained from cw-EPR measurements. Notably, these sharper, low-field features likely correspond to the spin-forbidden, $\Delta M_S = 2$ transitions, while the broader features originate from spin-allowed, $\Delta M_S = 1$. The nonzero echo intensity obtained for **1** and **2** demonstrate that multiple transitions in the spin manifold can be manipulated with coherent control.

We determined the spin–lattice relaxation time, T_1, the upper limit for information storage in a qubit, using a saturation recovery sequence (long pulse-T-$\pi/2$-τ-π-τ-echo). The magnitude of T_1 represents the lattice contribution to spin relaxation. We fit the saturation recovery curves with a monoexponential function, $I = -I_0(e^{T/T_1} - 1)$. At 5 K, the low- and high-field values ($\Delta M_S = 2$ and 1, respectively) of T_1 for **1** and **2** fall in the range 10–12 μs (Figure 3b). With increasing temperature, we find the temperature dependence of T_1 varies significantly as a function of field, and therefore transition identity. The values of T_1 for the $\Delta M_S = 1$ transitions have a greater temperature dependence, dropping precipitously from 5 to 7 K for fields > 0 T for **2**. At these low experimental temperatures, the field dependence of T_1 suggests the direct process is the dominant relaxation mechanism.[39−42] We attribute the more pronounced field dependence in **2** to the higher zero-field splitting values, which results in faster spin–lattice relaxation times.[43]

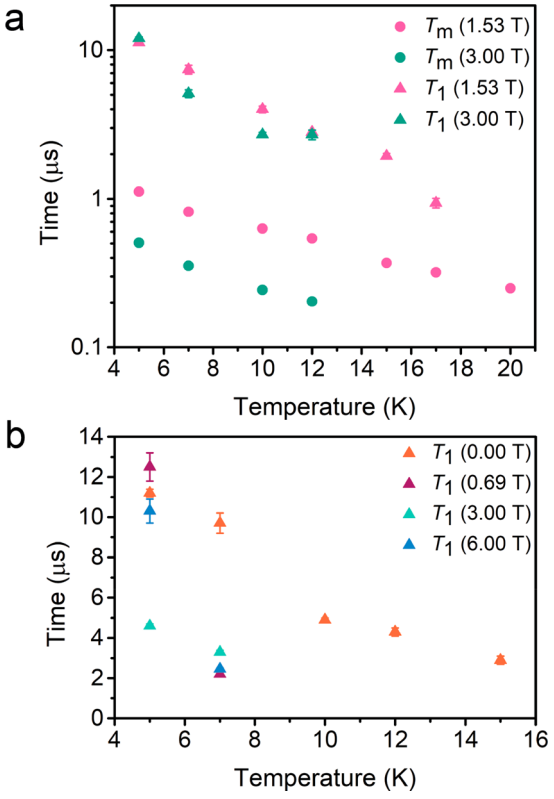

Figure 3. (a) T_1 and T_m values for **1** at 1.53 T (blue) and 3.00 T (pink). (b) T_1 values for **2** at zero field (0.00 T) and high fields (0.69, 3.00, and 6.00 T).

To assess the coherence properties of these molecules, we determined the phase memory time (T_m), which encompasses all processes that contribute to decoherence, including the electron spin T_2 and inhomogeneous dephasing time T_2*. Monoexponential functions ($I = I_0\, e^{-2\tau/T_m}$) were fit to the echo decays. For both **1** and **2**, T_m values decay rapidly with increasing temperatures. In line with the T_1 values, the $\Delta M_S = 1$ superpositions have a greater temperature dependence in comparison to the $\Delta M_S = 2$ transitions. In **1**, T_m at 1.53 T was 0.25(1) μs at 20 K, while there was no echo intensity above 15 K at 3.00 T, where T_m yielded a value of 0.072(8) μs. The convergence of T_1 and T_m at the higher temperatures establishes T_m is T_1-limited in **1** and **2**, at all investigated fields (Figure 3a), which has been observed in $S > 1/2$ metal complexes.[44,45] Despite the field dependence of the spin–lattice relaxation times, there is no dependence of field on the spin–spin relaxation times in **1** and **2**. While magnetic fields typically suppress intermolecular interactions by locking electronic spins in alignment with the field and thus increase T_m,[46] we attribute this finding to the 1 mM concentration where spin–spin interactions may be minor.

An optically addressable molecular qubit requires an emissive component as a readout mechanism for the spin information. Indeed, we selected these compounds for their strong field ligands that may enable emission. We acquired emission spectroscopy data by excitation with a 450 nm cw laser source. Powders of **1** and **2** produce broad emission at λ_{max} = 938–944 nm (Figures S25 and S26), satisfying the emissive readout criterion for an optically addressable molecular qubit. To elucidate the electronic excited state manifold, we acquired UV–vis data, basing our transition assignments on published computational analyses of **1** and **2**, albeit with different anions.[35,47] We observe a $^3A_{2g} \rightarrow {}^3T_{2g}$ transition along with a pronounced lower energy shoulder in the $^3T_{2g}$ band, which has been calculated and assigned as the spin-flip transition $^3A_{2g} \rightarrow {}^1E_g$.[48] The $^3A_{2g} \rightarrow {}^1E_g$ band does not shift in energy, but does lose intensity in **2**, consistent with the intensity borrowing mechanism observed in the electronic absorption spectra of octahedral nickel(II) complexes.[47] The methylene spacer in the pyr_3 ligand accommodates a larger bite angle and creates more overlap between the metal d orbitals and the ligands, relative to the phen derivative. Accordingly, we observe an increase in ligand field strength, in which the $^3A_{2g} \rightarrow {}^3T_{2g}$ transition blue-shifts by 400 cm^{-1} from **1** to **2**, in agreement with previous studies (Figure S24).[35,47]

Compounds **1** and **2** expand our molecular toolkit of spin qubits to nickel and represent, to the best of our knowledge, the first molecular Ni^{2+} qubit candidates. The combination of a transition that can be manipulated by pulse EPR spectroscopy coupled with emission suggests these air-stable compounds are viable candidates as optically addressable molecular qubits. Future research will focus on integrating these molecules with spectroscopic approaches designed to measure defect-based qubits.

■ ASSOCIATED CONTENT

Supporting Information

The Supporting Information is available free of charge at https://pubs.acs.org/doi/10.1021/jacs.0c06909.

https://dx.doi.org/10.1021/jacs.0c06909
J. Am. Chem. Soc. 2020, 142, 14826−14830

Full experimental and crystallographic details; additional spectroscopic and magnetic data (PDF)

AUTHOR INFORMATION

Corresponding Author

Danna E. Freedman − *Department of Chemistry, Northwestern University, Evanston, Illinois 60208, United States;* orcid.org/0000-0002-2579-8835; Email: danna.freedman@northwestern.edu

Authors

Michael K. Wojnar − *Department of Chemistry, Northwestern University, Evanston, Illinois 60208, United States*

Daniel W. Laorenza − *Department of Chemistry, Northwestern University, Evanston, Illinois 60208, United States*

Richard D. Schaller − *Department of Chemistry, Northwestern University, Evanston, Illinois 60208, United States; Center for Nanoscale Materials, Argonne National Laboratory, Lemont, Illinois 60439, United States;* orcid.org/0000-0001-9696-8830

Complete contact information is available at: https://pubs.acs.org/10.1021/jacs.0c06909

Notes

The authors declare no competing financial interest.

ACKNOWLEDGMENTS

We thank Drs. K. Kundu, A. Ozarowski, J. van Tol, L. Song, and Prof. S. Hill for fruitful discussions and experimental assistance, and T. J. Pearson, A. B. Altman, K. A. Collins, and C.-J. Yu for helpful comments on the manuscript. D.E.F., D.W.L., and M.K.W. acknowledge DE-SC0019356 for funding this research. A portion of this work was performed at the National High Magnetic Field Laboratory, which is supported by the National Science Foundation Cooperative Agreement No. DMR-1644779 and the State of Florida. This work made use of the IMSERC facility at Northwestern University, which has received support from Northwestern University, the State of Illinois, and the Int. Institute of Nanotechnology. Use of the Center for Nanoscale Materials, an Office of Science user facility, was supported by the U.S. Department of Energy, Office of Science, Office of Basic Energy Sciences, under Contract No. DE-AC02-06CH11357.

REFERENCES

(1) Maze, J. R.; Stanwix, P. L.; Hodges, J. S.; Hong, S.; Taylor, J. M.; Cappellaro, P.; Jiang, L.; Dutt, M. V. G.; Togan, E.; Zibrov, A. S.; Yacoby, A.; Walsworth, R. L.; Lukin, M. D. Nanoscale Magnetic Sensing with an Individual Electronic Spin in Diamond. *Nature* **2008**, *455*, 644−647.

(2) Dolde, F.; Fedder, H.; Doherty, M. W.; Nöbauer, T.; Rempp, F.; Balasubramanian, G.; Wolf, T.; Reinhard, F.; Hollenberg, L. C. L.; Jelezko, F.; Wrachtrup, J. Electric-Field Sensing Using Single Diamond Spins. *Nat. Phys.* **2011**, *7*, 459−463.

(3) Maletinsky, P.; Hong, S.; Grinolds, M. S.; Hausmann, B.; Lukin, M. D.; Walsworth, R. L.; Loncar, M.; Yacoby, A. A Robust Scanning Diamond Sensor for Nanoscale Imaging with Single Nitrogen-Vacancy Centres. *Nat. Nanotechnol.* **2012**, *7*, 320−324.

(4) Mamin, H. J.; Kim, M.; Sherwood, M. H.; Rettner, C. T.; Ohno, K.; Awschalom, D. D.; Rugar, D. Nanoscale Nuclear Magnetic Resonance with a Nitrogen-Vacancy Spin Sensor. *Science* **2013**, *339*, 557−560.

(5) Kucsko, G.; Maurer, P. C.; Yao, N. Y.; Kubo, M.; Noh, H. J.; Lo, P. K.; Park, H.; Lukin, M. D. Nanometre-Scale Thermometry in a Living Cell. *Nature* **2013**, *500*, 54−58.

(6) Degen, C. L.; Reinhard, F.; Cappellaro, P. Quantum Sensing. *Rev. Mod. Phys.* **2017**, *89*, 035002.

(7) Awschalom, D. D.; Hanson, R.; Wrachtrup, J.; Zhou, B. B. Quantum Technologies with Optically Interfaced Solid-State Spins. *Nat. Photonics* **2018**, *12*, 516−527.

(8) Atzori, M.; Sessoli, R. The Second Quantum Revolution: Role and Challenges of Molecular Chemistry. *J. Am. Chem. Soc.* **2019**, *141*, 11339−11352.

(9) Shiddiq, M.; Komijani, D.; Duan, Y.; Gaita-Ariño, A.; Coronado, E.; Hill, S. Enhancing Coherence in Molecular Spin Qubits via Atomic Clock Transitions. *Nature* **2016**, *531*, 348−351.

(10) Fataftah, M. S.; Krzyaniak, M. D.; Vlaisavljevich, B.; Wasielewski, M. R.; Zadrozny, J. M.; Freedman, D. E. Metal-Ligand Covalency Enables Room Temperature Molecular Qubit Candidates. *Chem. Sci.* **2019**, *10*, 6707−6714.

(11) Ferrando-Soria, J.; Moreno Pineda, E.; Chiesa, A.; Fernandez, A.; Magee, S. A.; Carretta, S.; Santini, P.; Vitorica-Yrezabal, I. J.; Tuna, F.; Timco, G. A.; McInnes, E. J. L.; Winpenny, R. E. P. A Modular Design of Molecular Qubits to Implement Universal Quantum Gates. *Nat. Commun.* **2016**, *7*, 11377.

(12) Nelson, J. N.; Zhang, J.; Zhou, J.; Rugg, B. K.; Krzyaniak, M. D.; Wasielewski, M. R. CNOT Gate Operation on a Photogenerated Molecular Electron Spin-Qubit Pair. *J. Chem. Phys.* **2020**, *152*, 014503.

(13) Yamabayashi, T.; Atzori, M.; Tesi, L.; Cosquer, G.; Santanni, F.; Boulon, M.-E.; Morra, E.; Benci, S.; Torre, R.; Chiesa, M.; Sorace, L.; Sessoli, R.; Yamashita, M. Scaling Up Electronic Spin Qubits into a Three-Dimensional Metal-Organic Framework. *J. Am. Chem. Soc.* **2018**, *140*, 12090−12101.

(14) Urtizberea, A.; Natividad, E.; Alonso, P. J.; Andrés, M. A.; Gascón, I.; Goldmann, M.; Roubeau, O. A Porphyrin Spin Qubit and Its 2D Framework Nanosheets. *Adv. Funct. Mater.* **2018**, *28*, 1801695.

(15) Cimatti, I.; Bondì, L.; Serrano, G.; Malavolti, L.; Cortigiani, B.; Velez-Fort, E.; Betto, D.; Ouerghi, A.; Brookes, N. B.; Loth, S.; Mannini, M.; Totti, F.; Sessoli, R. Vanadyl Phthalocyanines on Graphene/SiC(0001): Toward a Hybrid Architecture for Molecular Spin Qubits. *Nanoscale Horiz.* **2019**, *4*, 1202−1210.

(16) Yu, C.-J.; Krzyaniak, M. D.; Fataftah, M. S.; Wasielewski, M. R.; Freedman, D. E. A Concentrated Array of Copper Porphyrin Candidate Qubits. *Chem. Sci.* **2019**, *10*, 1702−1708.

(17) Childress, L.; Hanson, R. Diamond NV Centers for Quantum Computing and Quantum Networks. *MRS Bull.* **2013**, *38*, 134−138.

(18) Wu, Y.; Jelezko, F.; Plenio, M. B.; Weil, T. Diamond Quantum Devices in Biology. *Angew. Chem., Int. Ed.* **2016**, *55*, 6586−6598.

(19) Koehl, W. F.; Diler, B.; Whiteley, S. J.; Bourassa, A.; Son, N. T.; Janzén, E.; Awschalom, D. D. Resonant Optical Spectroscopy and Coherent Control of Cr^{4+} Spin Ensembles in SiC and GaN. *Phys. Rev. B: Condens. Matter Mater. Phys.* **2017**, *95*, 035207.

(20) Spindlberger, L.; Csóré, A.; Thiering, G.; Putz, S.; Karhu, R.; Hassan, J. U.; Son, N. T.; Fromherz, T.; Gali, A.; Trupke, M. Optical Properties of Vanadium in 4 *H* Silicon Carbide for Quantum Technology. *Phys. Rev. Appl.* **2019**, *12*, 014015.

(21) Bosma, T.; Lof, G. J. J.; Gilardoni, C. M.; Zwier, O. V.; Hendriks, F.; Magnusson, B.; Ellison, A.; Gällström, A.; Ivanov, I. G.; Son, N. T.; Havenith, R. W. A.; van der Wal, C. H. Identification and Tunable Optical Coherent Control of Transition-Metal Spins in Silicon Carbide. *Npj Quantum Inf.* **2018**, *4*, 48.

(22) Raha, M.; Chen, S.; Phenicie, C. M.; Ourari, S.; Dibos, A. M.; Thompson, J. D. Optical Quantum Nondemolition Measurement of a Single Rare Earth Ion Qubit. *Nat. Commun.* **2020**, *11*, 1605.

(23) Kindem, J. M.; Ruskuc, A.; Bartholomew, J. G.; Rochman, J.; Huan, Y. Q.; Faraon, A. Control and Single-Shot Readout of an Ion Embedded in a Nanophotonic Cavity. *Nature* **2020**, *580*, 201−204.

(24) Bayliss, S. L.; Laorenza, D. W.; Mintun, P. J.; Diler, B.; Freedman, D. E. Optically Addressable Molecular Spins for Quantum Information Processing. *arXiv:2004.07998*.

(25) Fataftah, M. S.; Freedman, D. E. Progress towards Creating Optically Addressable Molecular Qubits. *Chem. Commun.* **2018**, *54*, 13773−13781.
(26) Basolo, F.; Hayes, J. C.; Neumann, H. M. Mechanism of Racemization of Complex Ions. II. Kinetics of the Dissociation and Racemization of Tris-(1,10-Phenanthroline)-Iron(II) and Tris-(2,2′-Dipyridyl)-Iron(II) Complexes[1,2]. *J. Am. Chem. Soc.* **1954**, *76*, 3807−3809.
(27) Robinson, A.; Curry, J. D.; Busch, H. Complexes Derived from Strong Field Ligands. XVII. Electronic Spectra of Octahedral Nickel(II) Complexes with Ligands of the -Diimine and Closely Related Classes. *Inorg. Chem.* **1963**, *2*, 1178.
(28) Krzystek, J.; Ozarowski, A.; Telser, J. Multi-Frequency, High-Field EPR as a Powerful Tool to Accurately Determine Zero-Field Splitting in High-Spin Transition Metal Coordination Complexes. *Coord. Chem. Rev.* **2006**, *250*, 2308−2324.
(29) Azamat, D. V.; Badalyan, A. G.; Dejneka, A.; Jastrabik, L.; Lančok, J. Electron Spin-Lattice Relaxation of Low-Symmetry Ni^{2+} Centers in LiF. *Appl. Phys. Lett.* **2014**, *104*, 252902.
(30) Azamat, D. V.; Badalyan, A. G.; Dejneka, A.; Jastrabik, L.; Lančok, J. Zero-Field Studies of Spin-Lattice Relaxation Processes in Non-Kramers Doublet of LiF:Ni^{2+}. *Appl. Phys. A: Mater. Sci. Process.* **2016**, *122*, 1026.
(31) Titiš, J.; Boča, R. Magnetostructural *D* Correlation in Nickel(II) Complexes: Reinvestigation of the Zero-Field Splitting. *Inorg. Chem.* **2010**, *49*, 3971−3973.
(32) Maganas, D.; Krzystek, J.; Ferentinos, E.; Whyte, A. M.; Robertson, N.; Psycharis, V.; Terzis, A.; Neese, F.; Kyritsis, P. Investigating Magnetostructural Correlations in the Pseudooctahedral *Trans*-$[Ni^{II}\{(OPPh_2)(EPPh_2)N\}_2(Sol)_2]$ Complexes (E = S, Se; Sol = DMF, THF) by Magnetometry, HFEPR, and Ab Initio Quantum Chemistry. *Inorg. Chem.* **2012**, *51*, 7218−7231.
(33) Whangbo, M.-H.; Gordon, E. E.; Xiang, H.; Koo, H.-J.; Lee, C. Prediction of Spin Orientations in Terms of HOMO-LUMO Interactions Using Spin-Orbit Coupling as Perturbation. *Acc. Chem. Res.* **2015**, *48*, 3080−3087.
(34) Figgis, B. N.; Goodman, I. *Introduction to Ligand Fields*; Interscience Publishers: New York, 1966.
(35) Astley, T.; Hitchman, M. A.; Keene, F. R.; Tiekink, E. R. T. Structural, Spectroscopic and Angular-Overlap studies of Tripodal Pyridine Ligands with Nickel(II) and Zinc(II). *J. Chem. Soc., Dalton Trans.* **1996**, 1845−1851.
(36) Vander Griend, D. A.; Bediako, D. K.; DeVries, M. J.; DeJong, N. A.; Heeringa, L. P. Detailed Spectroscopic, Thermodynamic, and Kinetic Characterization of Nickel(II) Complexes with 2,2'-Bipyridine and 1,10-Phenanthroline Attained via Equilibrium-Restricted Factor Analysis. *Inorg. Chem.* **2008**, *47*, 656−662.
(37) Cruickshank, P. A. S.; Bolton, D. R.; Robertson, D. A.; Hunter, R. I.; Wylde, R. J.; Smith, G. M. A Kilowatt Pulsed 94 GHz Electron Paramagnetic Resonance Spectrometer with High Concentration Sensitivity, High Instantaneous Bandwidth, and Low Dead Time. *Rev. Sci. Instrum.* **2009**, *80*, 103102.
(38) Song, L.; Liu, Z.; Kaur, P.; Esquiaqui, J. M.; Hunter, R. I.; Hill, S.; Smith, G. M.; Fanucci, G. E. Toward Increased Concentration Sensitivity for Continuous Wave EPR Investigations of Spin-Labeled Biological Macromolecules at High Fields. *J. Magn. Reson.* **2016**, *265*, 188−196.
(39) Nellutla, S.; Morley, G. W.; van Tol, J.; Pati, M.; Dalal, N. S. Electron Spin Relaxation and K^{39} Pulsed ENDOR Studies on Cr^{5+}-Doped K_3NbO_8 at 9.7 and 240 GHz. *Phys. Rev. B: Condens. Matter Mater. Phys.* **2008**, *78*, 054426.
(40) van Tol, J.; Morley, G. W.; Takahashi, S.; McCamey, D. R.; Boehme, C.; Zvanut, M. E. High-Field Phenomena of Qubits. *Appl. Magn. Reson.* **2009**, *36*, 259−268.
(41) Zadrozny, J. M.; Graham, M. J.; Krzyaniak, M. D.; Wasielewski, M. R.; Freedman, D. E. Unexpected Suppression of Spin-Lattice Relaxation via High Magnetic Field in a High-Spin Iron(III) Complex. *Chem. Commun.* **2016**, *52*, 10175−10178.
(42) Jackson, C. E.; Lin, C.-Y.; Johnson, S. H.; van Tol, J.; Zadrozny, J. M. Nuclear-Spin-Pattern Control of Electron-Spin Dynamics in a Series of V(IV) Complexes. *Chem. Sci.* **2019**, *10*, 8447−8454.
(43) Raitsimring, A.; Dalaloyan, A.; Collauto, A.; Feintuch, A.; Meade, T. J.; Goldfarb, D. Zero Field Splitting Fluctuations Induced Phase Relaxation of Gd^{3+} in Frozen Solutions at Cryogenic Temperatures. *J. Magn. Reson.* **2014**, *248*, 71−80.
(44) Zadrozny, J. M.; Freedman, D. E. Qubit Control Limited by Spin-Lattice Relaxation in a Nuclear Spin-Free Iron(III) Complex. *Inorg. Chem.* **2015**, *54*, 12027−12031.
(45) Lenz, S.; Bamberger, H.; Hallmen, P. P.; Thiebes, Y.; Otto, S.; Heinze, K.; van Slageren, J. Chromium(III)-Based Potential Molecular Quantum Bits with Long Coherence Times. *Phys. Chem. Chem. Phys.* **2019**, *21*, 6976−6983.
(46) Takahashi, S.; Hanson, R.; van Tol, J.; Sherwin, M. S.; Awschalom, D. D. Quenching Spin Decoherence in Diamond through Spin Bath Polarization. *Phys. Rev. Lett.* **2008**, *101*, 047601.
(47) González, E.; Rodrigue-Witchel, A.; Reber, C. Absorption Spectroscopy of Octahedral Nickel(II) Complexes: A Case Study of Interactions between Multiple Electronic Excited States. *Coord. Chem. Rev.* **2007**, *251*, 351−363.
(48) Dorn, M.; Mack, K.; Carrella, L. M.; Rentschler, E.; Förster, C.; Heinze, K. Structure and Electronic Properties of an Expanded Terpyridine Complex of Nickel(II) $[Ni(Ddpd)_2](BF_4)_2$. *Z. Anorg. Allg. Chem.* **2018**, *644*, 706−712.

https://dx.doi.org/10.1021/jacs.0c06909
J. Am. Chem. Soc. 2020, 142, 14826−14830